ACTA SCIENTIAE

ISSN: 2178-7727

Green Synthesis of Size tunable CdSe Nanostructures for Bioapplications

Deepika, Nayandeep Mishra

Jyoti Vidyapeeth Womens University Jaipur, India
Author – dyadav969436@gmail.com
Corresponding Author – nayanmishra2007@gmail.com

ABSTRACT

Semiconductor quantum dots (QDs) have attracted sustained scientific and technological interest due to their size-dependent electronic structure, tunable optical properties, and strong quantum confinement effects. Among II–VI semiconductors, cadmium selenide (CdSe) quantum dots are particularly significant because of their narrow size distribution–dependent emission, high photoluminescence efficiency, and applicability in optoelectronic devices, bioimaging, photovoltaics, and light-emitting technologies. The present work aims to systematically investigate the structural, morphological, and optical properties of size-tunable and self-organized CdSe quantum dots synthesized using a cost-effective chemical bath deposition (CBD) technique in the presence of suitable surfactants. Emphasis is placed on understanding the correlation between synthesis conditions, nanocrystal size, crystallinity, surface morphology, and optical response.

The structural properties of the synthesized CdSe and CdSe/ZnSe quantum dots were examined using X-ray diffraction (XRD) analysis combined with Rietveld refinement, enabling accurate determination of crystallographic phase, lattice parameters, and crystallite size. Transmission electron microscopy (TEM) was employed to directly visualize particle morphology, size distribution, and core–shell architecture. Surface topography and nanoscale roughness of the deposited thin films were investigated through Raman spectroscopy, atomic force microscopy (AFM), providing both two-dimensional (2D) and three-dimensional (3D) morphological insights. Optical characteristics were evaluated using ultraviolet–visible (UV– Vis) absorption spectroscopy and photoluminescence (PL) spectroscopy under in-situ monitoring conditions to capture size-dependent absorption edge shifts and emission behavior.

The results demonstrate a pronounced quantum confinement effect, evidenced by a systematic blue shift in the absorption edge and band gap energy with decreasing particle size. Comparative analysis of particle size estimated from XRD, high-resolution AFM, and TEM revealed close agreement, confirming the reliability of the synthesis and characterization approach. The average particle sizes were found to be approximately 2.4, and 1.6 nm for CdSe quantum dots, and 2.6, nm for CdSe/ZnSe core–shell nanostructures, respectively. Photoluminescence spectra exhibited sharp band-edge emission with minimal Stokes shift, indicating high crystallinity and low defect density, while broader red-shifted emission components were attributed to surface or trap-state recombination processes.

KEYWORDS: Quantum dots; Cadmium selenide; Zinc selenide; Core shell nanostructure; Chemical bath deposition; Quantum confinement; Optical properties; Photoluminescence; TEM, AFM, RAMAN, Antimicrobial studies.

INTRODUCTION

The emergence of semiconductor nanocrystals, commonly referred to as quantum dots (QDs), has revolutionized the understanding of size-dependent physical phenomena in low- dimensional systems. When the dimensions of a semiconductor crystal approach or fall below the exciton Bohr radius, quantum confinement effects dominate, leading to discrete electronic energy levels and tunable optical properties that differ fundamentally from those of bulk materials. These effects make quantum dots uniquely suited for applications requiring precise control over absorption and emission wavelengths, including light-emitting diodes, lasers, photodetectors, solar cells, and biological labelling.

DOI: 10.22178/acta.26.1.33

ISSN: 2178-7727

Nanocrystals are generally classified based on the degree of carrier confinement: quantum wells (one-dimensional confinement), quantum wires (two-dimensional confinement), and quantum dots (three-dimensional confinement). Among these, quantum dots exhibit the most pronounced quantum size effects because both electrons and holes are confined in all three spatial dimensions (Brus, 1986). As a consequence, a reduction in particle size leads to a significant blue shift of the absorption edge, often spanning several electron volts, allowing optical tunability from the ultraviolet to the near-infrared region (Efros & Efros, 1982). Additionally, quantum confinement results in the transformation of continuous energy bands into discrete states, enhanced excitonic transitions at room temperature, slowed carrier relaxation, and modified electron–phonon interactions.

Cadmium selenide (CdSe) is one of the most extensively studied II–VI semiconductor materials owing to its direct band gap, high absorption coefficient, and well-established synthesis chemistry. CdSe quantum dots typically exhibit sharp band-edge photoluminescence with small Stokes shifts, arising from radiative recombination of confined electron–hole pairs (Norris et al., 1996). However, the presence of surface defects and trap states can introduce broader, red-shifted emission bands associated with non-radiative or trap-mediated recombination pathways, including Auger processes (Klimov, 2000). Understanding and controlling these recombination mechanisms is critical for optimizing quantum dot performance in optoelectronic applications.

The relaxation dynamics of photoexcited carriers in quantum dots involve multiple competing processes. Upon photon absorption, an electron is excited to higher energy states above the band gap, followed by rapid non-radiative vibrational relaxation to the lowest excited state on a picosecond timescale. Subsequent radiative recombination produces fluorescence emission, while alternative pathways such as carrier trapping or non-radiative relaxation can reduce emission efficiency (Bawendi et al., 1990). Surface passivation, often achieved through core–shell architectures, plays a vital role in suppressing trap states and enhancing photoluminescence quantum yield.

The synthesis of high-quality quantum dots with controlled size, narrow size distribution, and high crystallinity remains a central challenge in nanomaterials research. Various synthesis techniques, including molecular precursor routes, hot-injection methods, sol–gel processing, spray pyrolysis, and sonochemical approaches, have been reported (Murray et al., 1993; Peng et al., 2000). While these methods can produce highly monodisperse nanocrystals, they often require high temperatures, complex equipment, or stringent reaction control, limiting large- scale applicability.

In contrast, aqueous chemical routes such as chemical bath deposition offer significant advantages in terms of simplicity, low cost, scalability, and room-temperature processing (Lokhande et al., 2004). In CBD, parameters such as precursor concentration, pH, temperature, and capping agents can be precisely tuned to control nucleation and growth kinetics, enabling the synthesis of stable, monodisperse quantum dots with tailored properties. Despite these advantages, comprehensive studies correlating structural, morphological, and optical characteristics of CBD-grown CdSe quantum dots remain limited.

In this context, the present work focuses on the synthesis of size-tunable CdSe quantum dots using chemical bath deposition and their systematic characterization using X-ray diffraction, atomic force microscopy, transmission electron microscopy, UV–Vis absorption spectroscopy, and photoluminescence analysis. By establishing correlations between nanocrystal size, surface morphology, and optical behavior, this study aims to advance the understanding of self-organized quantum dot growth and provide insights relevant to the development of efficient nanoscale optoelectronic materials.

RESEARCH METHODOLOGY

2.1 Materials and chemical bath deposition chemistry

DOI: 10.22178/acta.26.1.33

ISSN: 2178-7727

Cadmium selenide quantum dots were synthesized using an aqueous chemical bath deposition (CBD) technique, which relies on controlled ion release, heterogeneous nucleation, and self-limited growth of nanocrystals on suitable substrates. Analytical-grade cadmium salt (typically cadmium acetate or cadmium sulfate) served as the Cd^{2+} source, while selenium was introduced through a chalcogenide precursor generated in situ from sodium selenosulfate under alkaline conditions. As a suitable surfactant tulsi plant extract was incorporated into the reaction bath to regulate particle growth, prevent agglomeration, and stabilize the nanocrystal surface.

In a typical deposition process, the cadmium precursor was dissolved in deionized water under constant magnetic stirring to ensure homogeneity. Complexing agents such as ammonia or triethanolamine were added gradually to control the free Cd^{2+} ion concentration through complex formation, thereby slowing down the nucleation rate. The selenium precursor solution was prepared separately and added dropwise to the cadmium-containing bath. The pH of the bath was carefully maintained in the alkaline range, as pH plays a critical role in determining the rate of ion release, nucleation density, and final particle size (Lokhande et al., 2004).

2.2 Nucleation and growth mechanism of CdSe and CdSe/ ZnSe quantum dots

The growth mechanism of CdSe quantum dots in the CBD process can be described in terms of classical nucleation theory coupled with diffusion-controlled growth. Initially, supersaturation is achieved through the slow release of Cd^{2+} and Se^{2-} ions, leading to the formation of CdSe nuclei once the ionic product exceeds the solubility product of CdSe.

These nuclei act as seeds for subsequent growth. The presence of surfactant molecules adsorbed on the nanocrystal surface selectively binds to high-energy facets, reducing surface energy and inhibiting uncontrolled growth. As deposition proceeds, growth becomes self- limited due to the depletion of reactive species and steric hindrance imposed by the capping layer. This results in narrow size distributions and enhanced size tunability. The competition between nucleation and growth stages is critically influenced by bath temperature, precursor concentration, and deposition time. Lower temperatures and higher complexing strength favor nucleation-dominated regimes, yielding smaller quantum dots, whereas elevated temperatures promote growth-dominated regimes and slightly larger particle sizes.

To improve optical stability and reduce surface trap states, core–shell structures such as CdSe/ZnSe were fabricated by sequential deposition. In the conventional CdSe/ZnSe configuration, a thin ZnSe shell was deposited over the CdSe core by introducing zinc and se precursors into the bath after CdSe nucleation. The wider band gap ZnSe shell provides effective surface passivation, suppressing non-radiative recombination and enhancing photoluminescence efficiency (Peng et al., 2000). Self-assembled CdSe nanocrystals are synthesized from Cd and elemental Se precursors using a wet chemical method where particle size depends on reaction time, temperature, precursor's concentration and capping agents etc. At first, in a typical synthesis procedure, the glass substrates used for deposition of CdSe quantum dots were cleaned in Extron solution followed by ultra-sonifically cleaning. The selenium ion precursor was prepared from a stock solution of sodium selenosulphite(Na2SeSO3). For this purpose Na2SO3 and elemental selenium in a molar ratio of 1:2have been mixed at 40oC for 24 hours to form clean solution. CdSe quantum dots were synthesized in 35-40oC temperature comprising of sodium selenosulphite, cadmium chloride, tri-ethanolamine and hydrazine hydrate. Cadmium ion sources were provided by cadmium chloride, dissolved in an aqueous solution of trichloro-ethanol-amine and hydrazine hydrate. The pH of the reaction matrix was adjusted to 11 with the help of ammonia solution. The size of the CdSe quantum dots was controlled by adding an appropriate concentration of 2- mercaptoethanol(C2H6OS) as a capping agent in reaction matrix.

Colloidal CdSe quantum dots were prepared by chemical method in aqueous solution according to the following reactions [55,56].

DOI: 10.22178/acta.26.1.33

ISSN: 2178-7727

$$Cd^{2+} + 2OH^- + SeSO_3^{2-} \rightarrow CdSe + SO_4^{2-} + H_2O \quad \text{---------- (1)}$$

The colloidal CdSe nanocrystals were collected after 2.5 hours of growth and washed several times with triple distilled water. The values of synthesis parameters have been listed in table 1.

Table 1. A summary of synthesis parameters used for the preparation of CdSe quantum dots.

S.No.	Sample Name	Cappant /Se ratio	Particle size(nm)	Colour of as deposited CdSe
1	Sample A	0:1(pure)	5.5	Light Red
2	Sample B	1:1	2.5	Greenish Yellow
3	Sample C	1.2:1	2.1	Greenish Yellow
4	Sample D	1.5:1	1.6	Cream

The size of the quantum dots was controlled with the addition of appropriate quantities of Tulsi extract in the deposition matrix.

2.3 Characterization techniques

Structural and morphological properties were carried out by X-Ray diffraction (Shimadzu X- ray diffractrometer) with Rietveld refinement analysis, transmission electron microscopy (TEM-TECHANI-20-G2) RAMAN spectroscopy and atomic force microscopy (AFM- Shimadzu SPM 9500J2), Optical properties were also investigated using UV-vis spectroscopy (Shimadzu UVPC1601) and PL spectroscopy (Perkin ElemerLS-55, luminescence spectrometer). Structural analysis was carried out using X-ray diffraction (XRD) with Cu Kα radiation. Rietveld refinement was employed to extract precise lattice parameters, crystallite size, and phase purity. Surface morphology and nanoscale roughness were examined using atomic force microscopy (AFM) in tapping mode, providing both two- dimensional and three-dimensional surface profiles. Transmission electron microscopy (TEM) was used to directly determine particle size, shape, and core–shell structure. Optical properties were investigated using UV–Vis absorption spectroscopy to determine band gap energies and photoluminescence spectroscopy to analyze emission behavior and recombination pathways.

RESULTS AND DISCUSSION

3.1 Structural Properties

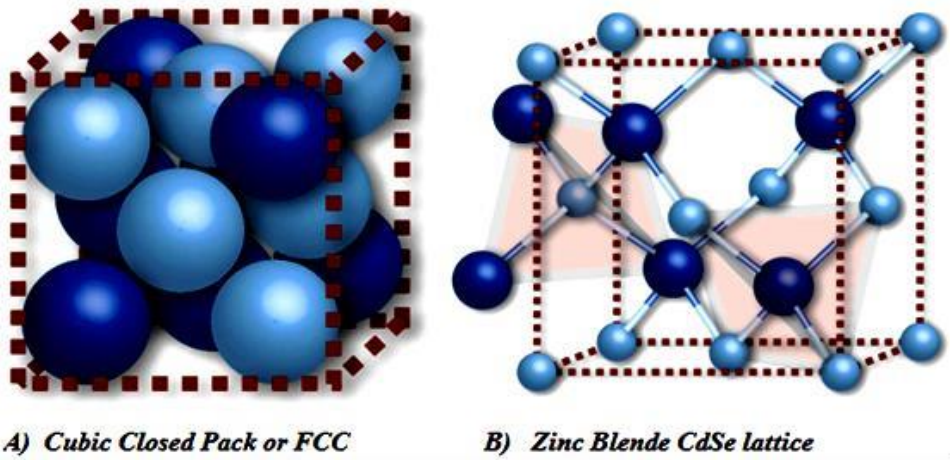

Figure 1. (A) Cubic closed packed structure and (B) Zinc blend CdSe

DOI: 10.22178/acta.26.1.33

ISSN: 2178-7727

Figure 1 (B) shows the unit cell of CdSe zinc blend nanocrystal. The large size nanocrystals of CdSe possess a hexagonal structure, whereas small nanocrystals seem to be in the cubic phase [57]. The solid blue spheres in the diagram denote Se- atom and sky-blue spheres denote Cd+ atoms. Cubic CdSe structure results when Cd+ atoms are placed on one FCC lattice and Se- atoms in the other FCC lattice. The conventional unit cell is a cube. The general position of the atom is a/4, a/4, a/4 parallel to the central axis mirror plane i.e. glides plane. Each unit cell consists of 4 anions and 4 cations. The axial and angular relationship of $\alpha=\beta=\gamma=90^{o}$ in CdSe gives it a characteristic symmetry of four 3-fold axes. The space group for CdSe is given by 'F43m', where 'F' and 'm' stands for 'FCC' and mirror symmetry respectively. The crystal structure of semiconductor nanocrystals can vary depending on the temperature, pressure, monomer concentration and type of legend used during the colloidal synthesis [35]. In the case of CdSe nanocrystals, there are three different structural forms that exist, zinc-Blende (cubic), wurtzite(hexagonal), and rock-salt (cubic) [46-54].

3.1.1 X-ray diffraction and Rietveld refinement.

X-ray diffraction patterns of the synthesized CdSe quantum dots confirmed the formation of a crystalline II–VI semiconductor phase with characteristic diffraction peaks corresponding to the hexagonal wurtzite structure. The observed broadening of diffraction peaks is indicative of nanoscale crystallite dimensions, consistent with quantum dot formation. Rietveld refinement enabled accurate estimation of crystallite size and lattice strain, revealing average sizes in the range of 2–3 nm, in good agreement with electron microscopy results. Minor peak shifts relative to bulk CdSe were attributed to lattice contraction induced by quantum confinement and surface stress effects (Brus, 1986).

We have carried out X-ray diffraction (XRD) studies on Cadmium selenide(CdSe) nanocrystals thin films grown on glass substrates by chemical bath deposition techniques.
The observed X-ray diffraction spectrums of a poly CdSe-A as well as three nanocrystals CdSe samples B, C and D grown using increasingly higher concentration of C2H6OS has been shown in Figure 2 (a) respectively. The observed peak positions, corresponding d-values, relative intensities, Miller planes and the calculated lattice parameter values along with standard JCPDS #190191 data of all the samples have been summarized in Table 2 (a). The standard JCPDF data for cubic CdSe has given in figure3. The broadening of the X-ray diffraction peak positions obtained from CdSe samples A to sample D implied a simultaneous reduction in the nanocrystals size for increasingly higher concentration of capping agent. In the figure 3.2 (a), the upper spectrum of CdSe sample A thin film exhibited three peaks positioned at 2θ = 25.50, 42.30 and 49.60 corresponding to d-values 3.53Å, 2.17Å and 1.85Å respectively. These X-ray diffraction peak positions correspond to the (111), (220) and (311) planes of the cubic phase of nanocrstalline sample CdSe-A and the measured value of lattice constant were 6.19 Å. The wurtzite phase of CdSe exhibit several peaks between 23.900 and 55.840 while the cubic phase is marked by only four peaks positioned at 2θ = 25.370, 42.040, 49.740 and 60.990. The occurrence of the wurtzite phase, owing to the existence of multiple peaks, could give rise to an asymmetric line shape of the X-ray diffraction spectra. The X-ray diffraction peaks of CdSe-B, CdSe-C and CdSe-D quantum dots samples are considerably broadened due to reduction in particle size. In all samples, the strongest XRD peak corresponded to reflection from (111) planes and the relative intensities of diffraction from (220) and (311) planes were weak indicating a preferred (111) orientation. To ascertain the peak positions and d-values from the broadened reflexes, we fitted the peaks using Reitveld refinement. The results ofthe Rietveld refinement have also been shown in the figure 3.4 by solid Red lines. The peak-fittingprogram revealed asymmetric peak shape at the corresponding 2θ positions indicating zincblind phase of CdSe.Size dependent structural transition has also been reported in CdSe [43-45]. The particle size of CdSe sample was found to decrease systematically with increasing use of capping agent to selenium ratio in the growth matrix. The average particle size calculated from the Scherrer's broadening of the X- ray diffraction pattern and also by Rietveld analysis good agreement with the size calculated from TEM also shown for two samples of CdSe quantum dots sample B and sample D in the next section. The calculated average particle size from the Rietveld refinement was obtained as 5.5 nm, 2.5 nm, 2.1 nm and 1.6 nm for the sample CdSe-A, CdSe-B, CdSe-C and CdSe-D respectively.

DOI: 10.22178/acta.26.1.33

ISSN: 2178-7727

Figure 3.2 (b) and (C) represents the observed X-ray diffraction pattern of ZnS and ZnSe quantum dot samples. In ZnSe nanocrystals three diffraction peaks are observed at 2θ = 27.610, 45.250, ad 53.200 corresponding to (111), (200) and (311) planes of cubic phase. The average particle size of ZnSe quantum dot calculated from the Scherrer's broadening of the X- ray diffraction pattern good agreement with electron microscopy. The ZnS quantum dot sample also exhibited three peaks at 2θ= 28.730, 47.690 and 56.660 corresponding d-values 3.05Å, 1.84Å, and 1.57Å respectively. These peaks correspond to (111), (220) and (311) of cubic ZnS.

Table 2 summary of the X-ray diffraction data for the CdSe quantum dots with different particle size.

Sample Name	Grain Size(nm)	2□ Degree	FWHM	dvalues Stan(Å) Obs(Å)		(hkl)	Lattice Para. Å	Phase Assign
Sample A	~5.5	25.5	1.560	3.51	3.53	(111)	6.19	(Cubic)
		42.3	1.282	2.14	2.17	(220)		(Cubic)
		49.6	1.348	1.83	1.85	(311)		(Cubic)
Sample B	~2.5	25.7	2.996	3.51	3.51	(111)	6.10	(Cubic)
		42.9	3.549	2.14	2.17	(220)		(Cubic)
		49.7	5.375	1.83	1.83	(311)		(Cubic)
Sample C	~2.1	25.8	5.323	3.51	3.50	(111)	6.08	(Cubic)
		42.9	6.22	2.14	2.13	(220)		(Cubic)
		49.9	10.21	1.83	1.82	(311)		(Cubic)
Sample D	~1.6	25.6	5.822	3.51	3.49	(111)	6.05	(Cubic)
		42.5	7.22	2.14	2.11	(220)		(Cubic)
		49.7	13.30	1.83	1.83	(311)		(Cubic)

DOI: 10.22178/acta.26.1.33

ISSN: 2178-7727

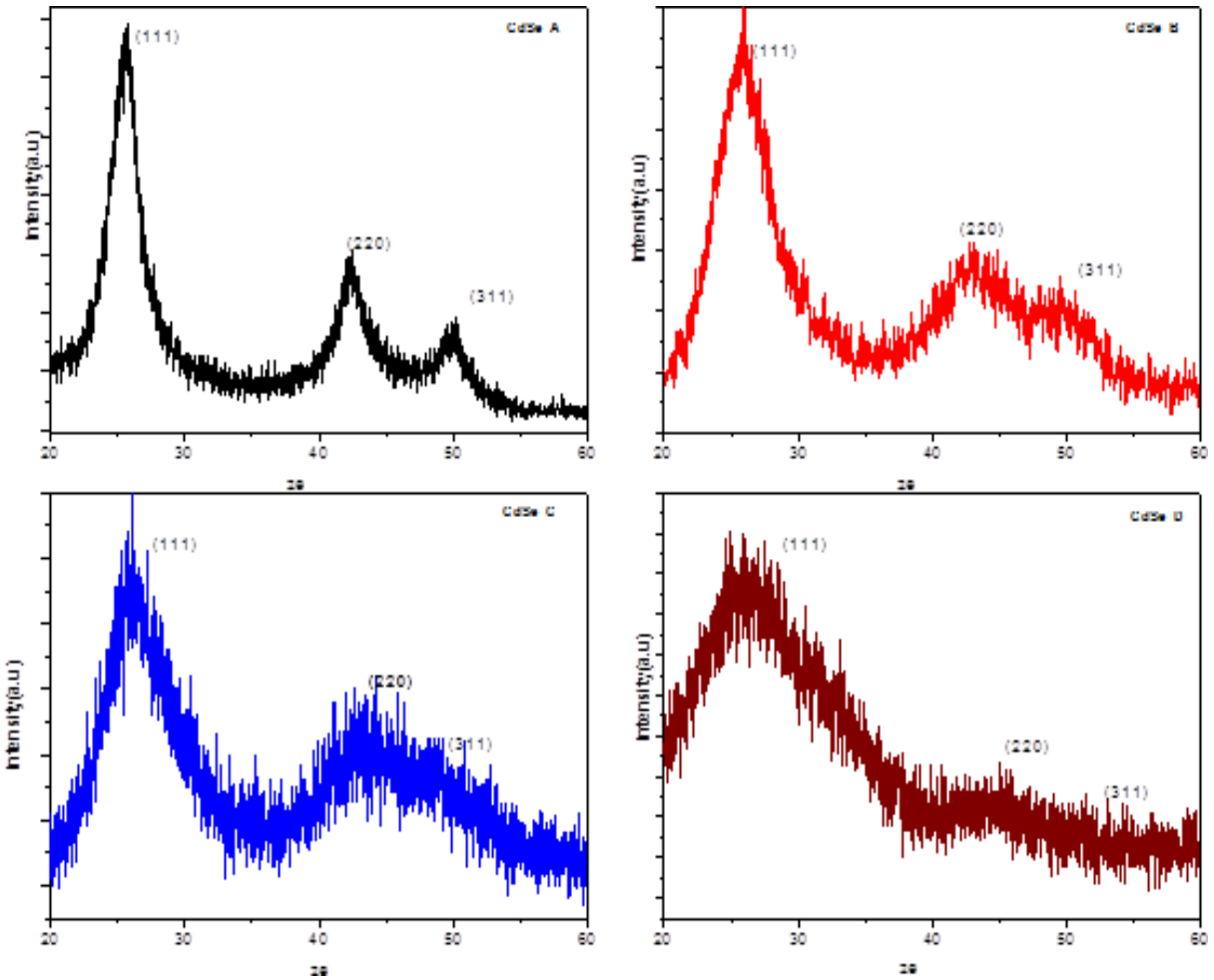

Figure 2. X-ray Diffraction patterns of CdSe Quantum Dots sample A, sample B, sample C, and sample D synthesized using 0.0, 1, 1.2 and 1.5 M mercapto respectively during growth.

DOI: 10.22178/acta.26.1.33

ISSN: 2178-7727

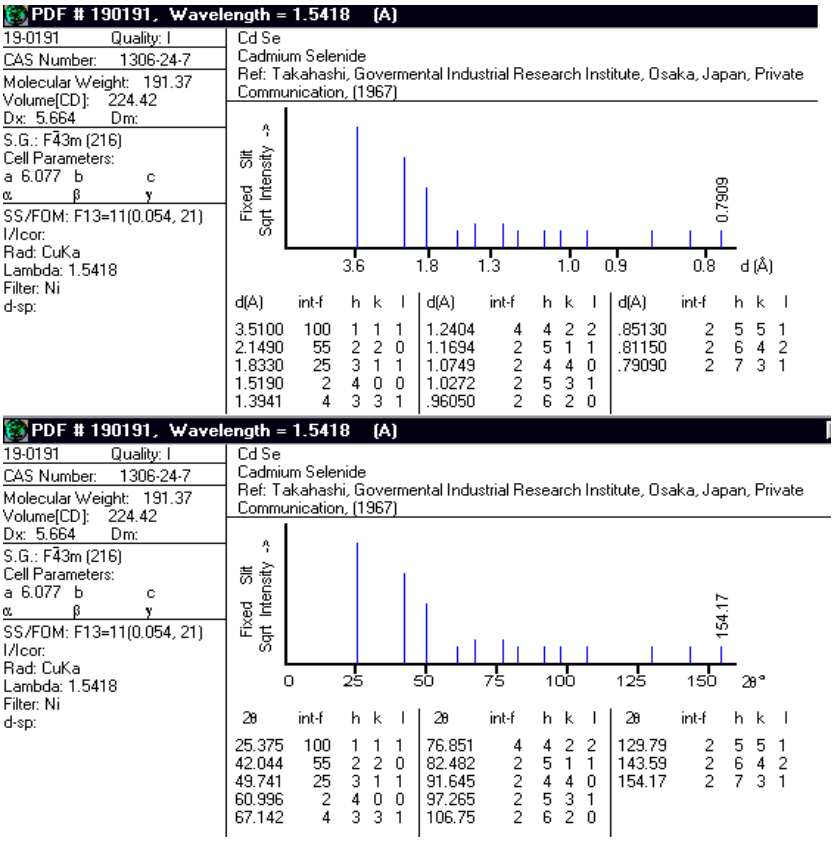

Figure 3.3 Zinc blende phase data of CdSe- JCPDS#19091

The calculated average particle size from the Scherrer's equation was obtained as 1.58 nm and 2.5 nm for the ZnS and ZnSe quantum dot samples respectively. In the Table 3.2 **(**b**)** the summary of XRD data for ZnSe and ZnS quantum dots is listed. The summary of the inter planer d-spacing along with corresponding peak intensities for CdSe semiconductor quantum dots are listed in Table 3.3

Table3.3 Summary of inter planer spacing and peak intensities of all CdSe.

Standard values		Cadmium selenide Quantum Dots CdSe								
d (Å)	I_{REL} (I/I_o)	Sample A		Sample B		Sample C		Sample D		(hkl)
		d (Å)	I_{REL} (I/I_o)	d (Å)	I_{REL} (I/I_o)	d (Å)	I_{REL} (I/I_o)	d (Å)	I_{REL} (I/I_o)	

DOI: 10.22178/acta.26.1.33

ISSN: 2178-7727

3.510 2.158 1.836	100 55 25	3.527 2.168 1.849	100 56 38	3.513 2.165 1.825	100 52 40	3.499 2.160 1.818	100 49 25	3.485 2.109 1.827	100 40 16	(111) (220) (311)

For accurate phase refinement or structural analysis of cubic CdSe, the observed XRD profiles are further refined with Rietveld analysis and results have been shown in figure 3.4. The observed experimental data (represented by white circled curves) are well matched with fitted profile (represented by red curve). The Bragg reflection on positions and marginal difference between observed and fitted profile (grey curves) have also been given in figure

3.4. We found that the light grey curve differences between experimentally observed and fitted profiles for all the samples were at approximately straight line and the goodness of fit (GOF) was very close to 1.5 indicating a reasonably good fitting [61-63]. The results of refinement such as space lattice, reliability factors (Chi2 and S), crystal parameters and crystalline volume have been tabulated in Table 3.4.

The obtained observations of Rietveld refinement of the CdSe samples structural data indicated a considerable compressive strain on the nanocrystals when the CdSe particle size decreased. Here we are discussing about the data refinement process in CdSe nanocrystals. The Rietveld refinement program DBWS-9411 is designed by R.A. Young et al [58-60] to carry out refinements with X-ray and neutron powder diffraction data in digitized form collected under any of several of the most commonly used instrumental conditions. The X- ray diffraction of CdSe nanocrystals samples-A to sample-D results in a pattern characterized by peaks in intensity at certain positions Rietveld refinement method uses least squares approach to refine a theoretical line profile until the best fit is obtained for the observed powder diffraction pattern known as DAT-file. Figure 3.5 shows the observed structure of 1.6NM CdSe quantum dot sampled by the Riteveld refinement visual studio. The solid pink spheres in the diagram denote Se- atom and blue spheres denote Cd+ atoms of Zinc Blend CdSe.This is accomplished by calculating pattern based on an input file known as PCR-file containing all the sample parameters, diffraction optics effects, instrumental factor, space- group occupancy, atomic position, temperature factors, pressure and strain etc. The description of our theoretical modelling methodology in the PCR file of CdSe samples for Nanocrystalline sample is shown below.

Table 4. Summary of the Rietveld refinement analysis for the CdSe quantum dots with different particle size.

Sample	Lattic Const ‘Å’	Space Group	X-Ray peak profile function	Size Distribution function	Numerical fit residuals		Gaussian Variance `Z``	GOF	χ^2	R_B	R_F	Part. size ‘Å’
					R_{wp}	R_{ex}						
Sam A	6.108	186	Pseudo	Gaussian	24.2	8.5	1.18	1.1	1.15	3.12	3.23	55
Sam B	6.070	186	Voit Pseudo	Gaussian	21.56	9.1	1.07	1.3	1.20	2.87	2.12	25

DOI: 10.22178/acta.26.1.33

ISSN: 2178-7727

Sam C	6.062	186	Voit	Gaussian	15.4	5.0	0.61	1.6	1.59	2.22	1.86	21
Sam D	6.049	186	Pseudo Voit Pseudo Voit	Gaussian	9.8	6.2	0.49	1.1	2.01	2.61	0.741	15.6

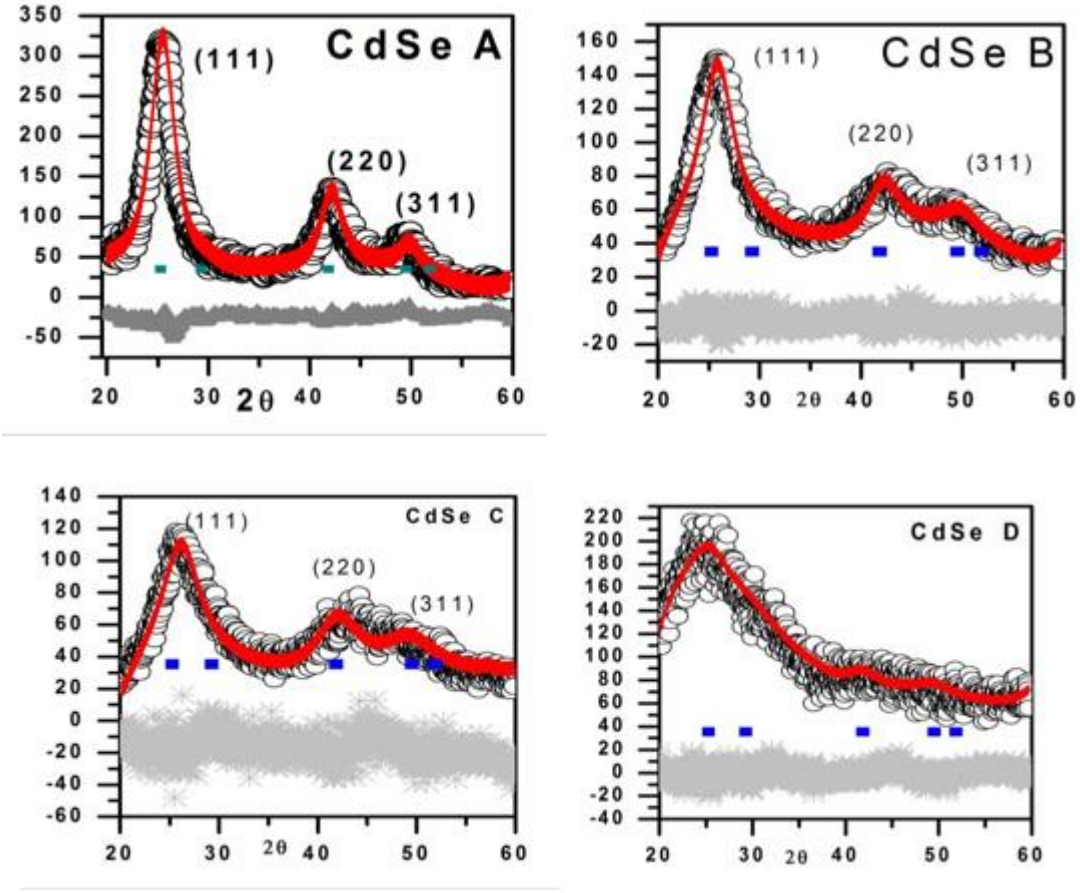

Figure 4. (a) X-ray Diffraction patterns with Rietveld refinement refinementof CdSe Quantum Dots (A) sample A [5.5nm] (b) Sample B [2.5nm] (c) Sample C [2.1nm] and

DOI: 10.22178/acta.26.1.33

ISSN: 2178-7727

(d) Sample D [1.6nm] in the as deposited conditions on glass substrate .The dark black curve with white circles corresponds to experimental diffraction pattern of the CdSe films, the solid red curve represents the calculated fitted data and light gray shows the difference between experimental observed and riteveld calculated results.

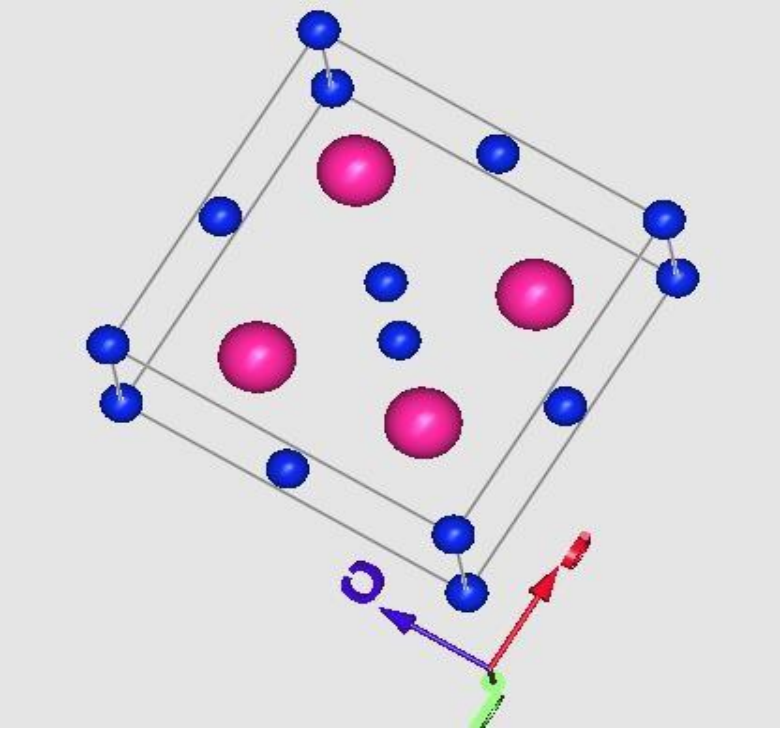

Figure 5. CdSe sample-D Rietveld refinement refine model structure.

Description of input file for CdSe nanocrystals: -
COMM CDSE 1.6nm
! Current global Chi2 (Bragg contrib.) = 1.968

! Files => DAT-file: CDSE 1.6nm, PCR-file: CDSE 1.6nm

!JobNprNphNbaNexNsc Nor Dum IwgIloIas Res SteNre Cry UniCor Opt Aut

0 5 1 0 0 0 0 0 0 0 0 0 1 0 0 0 0 0 0

!

!IprPplIoc Mat Pcr Ls1 Ls2 Ls3 NLI Prf Ins RpaSymHklFouSho Ana

0 0 0 0 2 0 4 0 0 1 0 0 0 0 0 1 0

!

! lambda1 Lambda2 Ratio BkposWdtCthmmuRAsyLimRpolarz -
>Patt# 1 1.540590 1.544400 0.5000 35.000 40.0000 0.7998 0.0000 50.00
0.0000
!

!NCYEpsR_atR_anR_prR_glThmin Step Thmax PSD Sent0

DOI: 10.22178/acta.26.1.33

ISSN: 2178-7727

1 0.01 0.99 0.99 0.99 0.99 20.0000 0.020000 60.0000 0.000 0.000

!

16 !Number of refined parameters

!

! Zero Code SyCos Code SySinCode Lambda Code MORE ->Patt# 1

-0.18374 20.0 0.00000 0.0 0.52024 190.0 0.000000 0.00 0

! Background coefficients/codes for Pattern# 1

89.997 -197.59 511.87 480.84 -2894.3 2538.7

31.000 41.000 51.000 61.000 71.000 81.000

!---------- ----------

! Data for PHASE number: 1 ==> Current R_Bragg for Pattern# 1: 17.51

!---------- ----------

CdSe

!

!Nat Dis Ang Pr1 Pr2 Pr3 JbtIrfIsyStr Furth ATZ NvkNpr More

2 0 0 0.0 0.0 1.0 0 0 0 0 0 12970.841 0 5 0

!

F -4 3 m <--Space group symbol

!AtomTyp X Y Z BisoOcc In Fin N_tSpc /Codes

Cd Cd+2 0.00000 0.00000 0.00000 0.00000 1.00000 0 0 0 0

0.00 0.00 0.00 0.00 0.00

Se Se-2 0.25000 0.25000 0.25000 0.00000 1.00000 0 0 0 0

0.00 0.00 0.00 0.00 0.00

!-------> Profile Parameters for Pattern # 1

! Scale Shape1 Bov Str1 Str2 Str3

DOI: 10.22178/acta.26.1.33

ISSN: 2178-7727

Strain-Model 0.22967E-06 1.57510 2.21914 0.00000 0.00000
0.00000 0
11.00000 130.001 140.001 200.000 210.000 220.000

! U V W X Y GauSizLorSiz Size-Model

31.516171 -10.372652 26.335419 0.002706 0.000000 2.025800 0.000000 0

110.001 120.001 100.001 160.000 0.000 150.000 0.000

! a b c alpha beta gamma #Cell Info

6.048766 6.048766 6.048766 90.000000 90.000000 90.000000

90.00000 90.00000 90.00000 0.00000 0.00000 0.00000

! Pref1 Pref2 Asy1 Asy2 Asy3
Asy4 0.00000 0.00000 0.00000
0.00000 0.00000 0.00000
0.00 0.00 171.00 181.00 0.00 0.00

! 2Th1/TOF1 2Th2/TOF2 Pattern to plot

20.000 60.000 1

The variance of the peak σ^2 varies with 2θ as,

$$\sigma^2 = U \tan(2\theta) + V\tan(\theta) + W + Z/\cos(2\theta) \text{ ---------- [3.4]}$$

Where, U, V and W are the coefficient described by Cagliotti, Pauletti and Ricci [64] and Z is the coefficient for Gaussian-Scherrerbroadening.The particle size **(Å)** is estimated by using the relation [65],

$$D = \frac{180\, C\, \lambda}{\pi \sqrt{8 In 2 Z}} \text{ ----------[3.5]}$$

The values of structural parameters (crystal system, space group lattice constant, Rp, Rwp, Rexp, RB, RF, $\chi 2$, D and S respectively) for CdSe nanocrystals have been listed in above Table 3.4. With the help of all Rietveld refinement parameters, we conclude that in the CdSe samples the lattice constant decrease continuously with the increase in the concentration of mercptoethanol or decrease in the particle radius. This reduction in lattice constant implies existence of compressive strain in the lattice of CdSe quantum dots. Mazher et al (2004) also reported this crystal lattice distortion phenomenon in II-VI group semiconductor quantum dots. [56]. This is clear from the CdSeRietveld refinement result that the quantum dots purely belong from only from Cubic phase these result also good agreement with the TEM diffraction results. Reitveld method also confirms the lattice parameter till 3rd decimal points accurately as well as d-values also. The high surface energy of CdSe nanocrystalline is the reason of presence of uniform strains in the films. Consequently, all the nanocrystals shall be plastically deformed to either tensile or compressive stress. This may cause shifts in the observed peak positions, d-values and lattice parameters. The goodness of fit and Z for all samples was between 0.5 and 1.6 indicating an accurate fitting model by Rietveld refinement

DOI: 10.22178/acta.26.1.33

ISSN: 2178-7727

software. The dependence of particle size with the variation in the capping agent to selenium ratio has been shown in figure 3.6. As shown in the figure, the quantum dots size and lattice parameter initially decreased with an increase in the molar concentration of capping agent in total volume of reaction matrix. The reduction in the lattice constant implies that the existence of compressive strain in CdSe semiconductor quantum dots. In the structural studies of CdSe quantum dots, particle size was found to decrease systematically with increasing use of capping agent to selenium ratio in the growth matrix.

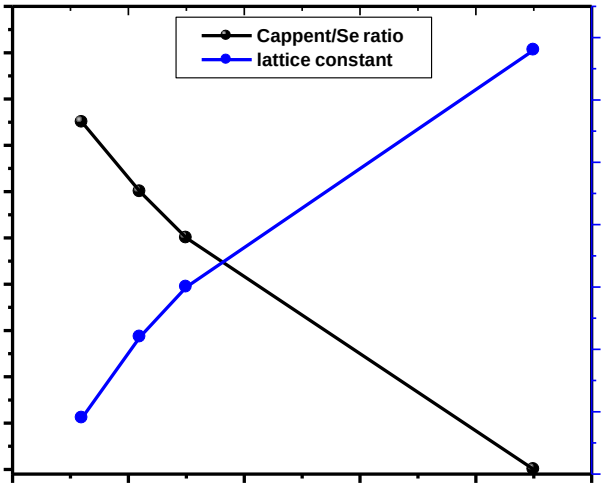

Figure: 6 Observed dependence of lattice constant '*a*' with particle size(black curve). In the blue curve the observed shift in particle size with mercapto/selenium ratio during the formation of nanocrystals CdSe. (Particle size in 'Å')

The dependence of particle size with the variation in the capping agent in selenium ratio has been shown in the blue curve of Figure 3.6. XRD results explain the role of capping agent in the quantum confinement process. The capping agent employed possesses a strong electron donor head group, its increasing concentration in the growth matrix, facilitated increasing adsorption on the growing CdSenanocrystallite surface resulting into reduction in particle size. It was, therefore, concluded that the capping agent used in the studies can effectively control the size of CdSe quantum dots.

3.3.1.3 Transmission Electron Microscopy

Transmission electron microscopy provided direct visualization of nearly spherical CdSe quantum dots with narrow size distribution. High-resolution TEM images showed clear lattice fringes, confirming high crystallinity. The measured particle sizes closely matched those estimated from XRD and AFM analyses, demonstrating the reliability of the CBD synthesis route. In core shell structures, contrast variation between core and shell regions further confirmed successful shell formation and interface integrity.

Figure 3.7 **(**a**)** and **(**b**)** represents TEM images obtain from CdSe-D and **(**c**)** and **(**d**)** are the typical TEM image from CdSe-B. Obviously the both samples of cadmium selenide quantum dots have spherical morphology and are almost homogeneously distributed. The size distribution histogram of the quantum dots sample CdSe-D and sample CdSe-B has been shown in figure 3.7 **(**e**)** and **(**f**)** respectively. A majority of nanocrystals was found to possess size of ~1.6nm and ~2.5nm respectively for CdSe-D and CdSe-B. The particle sizes estimated by TEM are in close agreement with the average particle size estimated using XRD. The calculated size dispersion was ~10%, which is a reasonably good achievement as summarized in the Table 3.5. The selective area diffraction pattern as shown in figure 3.8 revealed diffraction spots superimposed on a ring pattern, which indicated highly oriented crystal structure. The obtained diffraction pattern of CdSe-D figure 3.8 showed characteristic circular diffraction patterns corresponding to **(**111**)**, **(**220**)**, and **(**311**)** planes with

DOI: 10.22178/acta.26.1.33

ISSN: 2178-7727

d-values
3.507 Å, 2.141 Å and 1.83 Å respectively, of cubic phase of CdSe quantum dots sample. [66] The diffraction rings are broad and continues nature indicating the highly nanocrystalline nature of the sample-D. An area of the **(**111**)** diffraction ring in figure 3.8(A) was used to acquire a bright field image of the samples-D. The quantum dots were shown to possess a narrow size distribution. Figure 3.8 (B) shows the highly crystalline CdSe single phase core quantum dots. The analysis of diffraction pattern showed at the quantum dots conforms to rock salt cubic structure system. In CdSe-D sample **(**111**)** peak is most prominent or preferred orientation plane but (222),(002),(220) etc. planes also indicating in the pattern by red color.

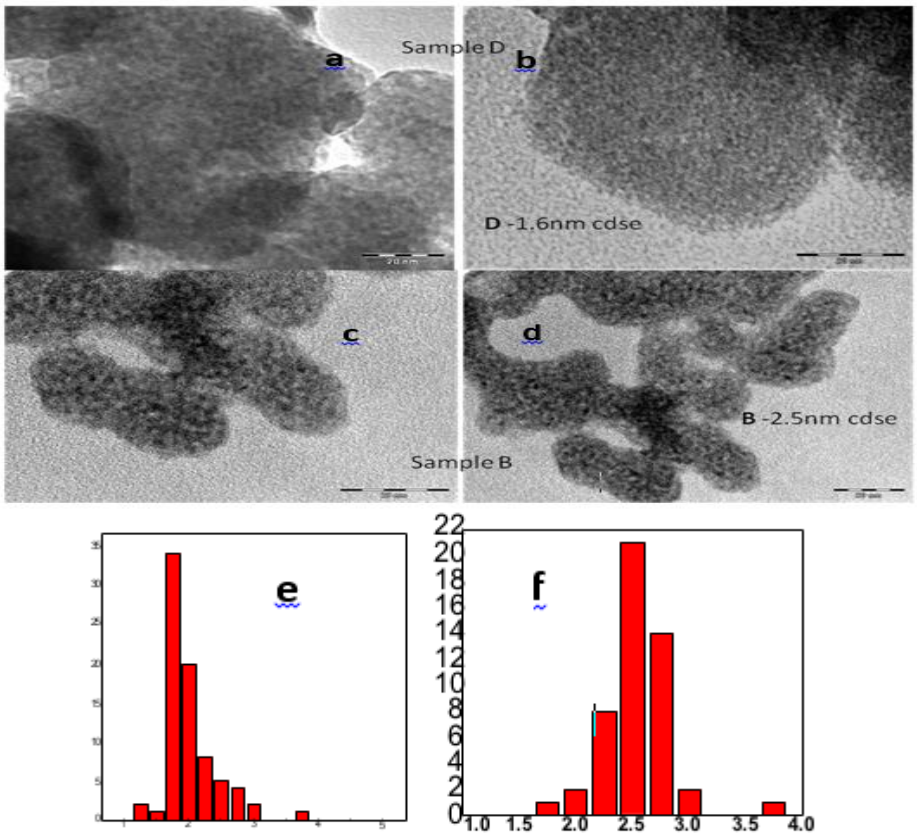

Figure 7. (a and b) The observed bright field TEM image of 1.6nm size CdSe sample-D. and (c. and d.) The observed bright field TEM image of 2.5nm size CdSe sample-B. (e. and f.). The particle size distribution histogram in CdSe samples-D (e) and sample-B (f)

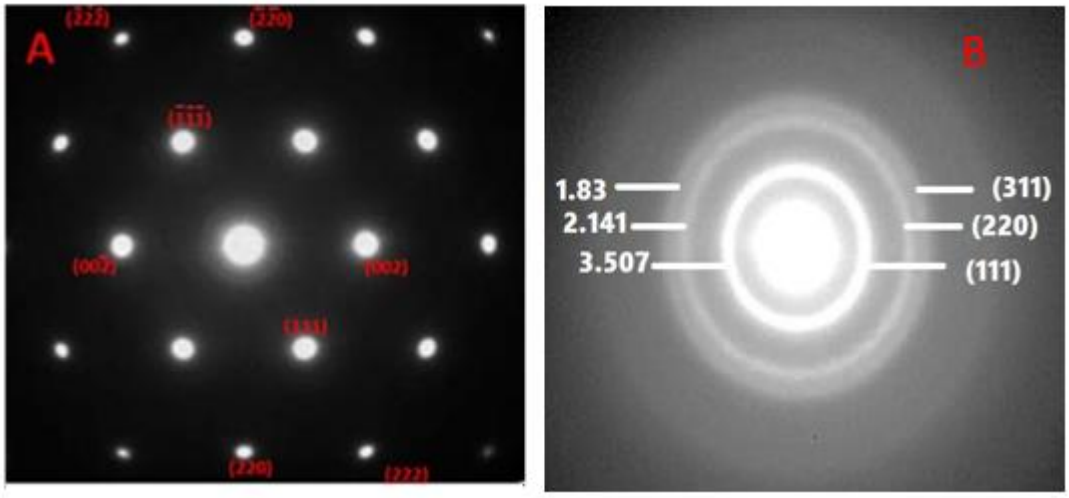

Figure: 8. (A) Diffraction pattern of CdSe-D quantum dots sample. The planes and d- values observed in diffraction pattern are also marked in the figure. (B) Lave pattern for CdSe-D

DOI: 10.22178/acta.26.1.33

ISSN: 2178-7727

Table 5 Comparison of estimated particle size, hkl and d-values of CdSe samples B and D by TEM and XRD.

Sample	Particle Size estimated by TEM	Average Particle Size estimated by XRD and Rietveld refinement analysis	hkl and d-values estimated by TEM		hkl and d-values estimated by XRD and Rietveld refinement analysis		Standard d-values (Å)
			hkl	d-value	hkl	d-value	
Sample B	2.5	~2.5	111	3.51	111	3.504	3.510
			220	2.15	220	2.165	2.149
			311	1.83	311	1.827	1.833
Sample D	1.65	~1.6	111	3.51	111	3.519	3.510
			220	2.14	220	2.109	2.149
			311	1.83	311	1.825	1.833

3.3.1.3 Raman Spectroscopy

The three CdSe quantum dots samples were analysed by Raman spectroscopic technique.The phonon study in CdSe is interesting, because the electron phonon coupling plays a critical role in the nanocrystals optical systems. The spectra were recorded in the range 150 to 800 cm^{-1}. Typical Raman scattering spectra of CdSe - A, CdSe-C and CdSe-D thin films samples are shown in Figure 9. The peak at 206 cm^{-1} is due to the longitudinal optical phonon mode (LO) of poly CdSe-A [67]. The phonon frequency of the longitudinal optical 2LO mode of CdSe at was found at 408 cm^{-1}. The LO phonon peak in the nanocrystalline Samples were slightly shifted to lower wave numbers. For example, for sample A, the LO phonon peak was positioned at 206 cm^{-1}. Also, the shape of the peaks acquired a shifting asymmetric shape for smaller nanocrystals. In nanocrystalss these effects may be observed due to the effect of strain. Note that the Raman peak of the 5.5nm Cdse quantum dots sample A considerably narrower and intense compared to a corresponding spectrum of other noncrystallineCdSe samples-C and sample-D. This result implies the presence of some amorphous phase in the nano size CdSe samples. Several interesting particle size dependent features in the spectra are shown. As particle size of CdSe decreases the line width broadens. The peak positions and FWHM of all observed Raman spectrum CdSe peaks is summarized in Table6. The FWHM of the 2LO peak in CdSe nanocrystals increased with decreasing particle size and from the spectum also observed that red shifted 2LO corespoending large particle size samples. In review articles the fundamental first-order, Raman band is located around 200 cm^{-1}. The band has an asymmetric shape, which is common for low-dimensional CdSe structures [68,69] and similar materials. Gupta et al. performed Raman measurements of GaP nanowires, which are similar to the CdSenanorods, in various dielectric surroundings and were able to verify the nature of the low-frequency shoulder and demonstrate the dependence on the surrounding [70]. At larger wavenumbers, around 400 cm^{-1}, the second-order Raman band can be observed. The relative intensity of the second-order band to the fundamental Raman band depends on the coupling strength between the phonons and excited charge carriers.InCdSenanocrystals, the phonon wavefunction is restricted to the volume of the nanocrystal. A model for confined phonons was initially developed by Richter et al. and applied for low-dimensional silicon nanocrystals[71].Finally observation from Raman characterization is the increased asymmetric broadening in the high- energy side of the Raman peaks for nanosrystlline samples, which may be assigned to the localization of phonon wave function within the quantum dots.

DOI: 10.22178/acta.26.1.33

ISSN: 2178-7727

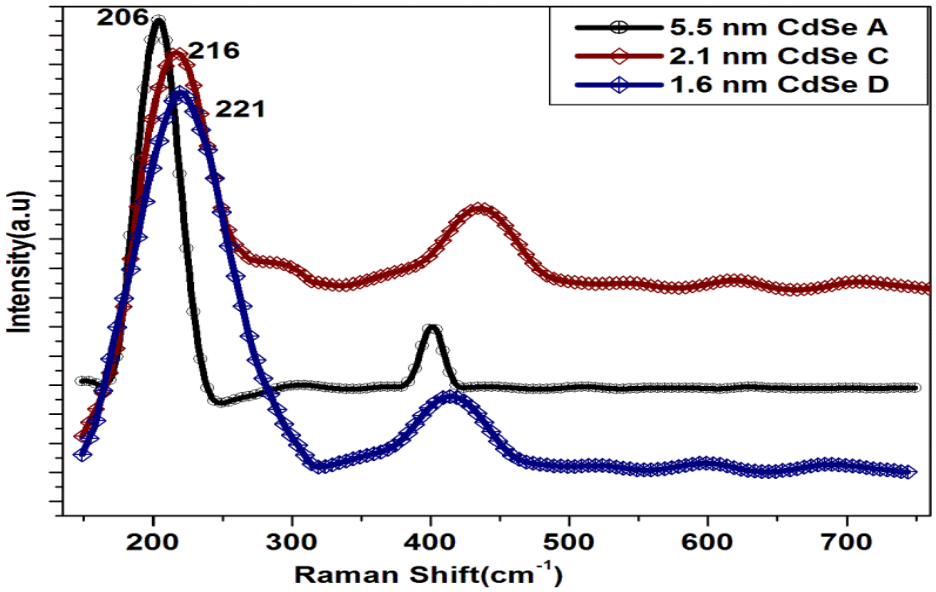

Figure: 9 Raman spectra (A, C and D) of CdSe thin films of samples A(5.5nm), C(2.1nm) and D(1.6nm).

Table 6 Raman Peak position and FWHM of CdSe thin films of samples A(5.5nm), C(2.1nm) and D(1.6nm).

Sample	Peak Position (/cm^{-1})		FWHM (/cm^{-1})	
	1LO	2LO	1LO	2LO
A(5.5nm)	206	408	22	13
C(2.1nm)	216	429	26	21.5
D(1.6nm)	221	431	35	-

3.1.5 Morphological Studies Atomic Force Microscopy

Atomic force microscopy images revealed uniform, densely packed nanostructured films with low surface roughness. The two-dimensional AFM images showed homogeneous grain distribution without evidence of large-scale agglomeration, while three-dimensional images highlighted nanoscale protrusions corresponding to individual or clustered quantum dots. The root mean square roughness values were found to be in the nanometer range, confirming the smooth and compact nature of the deposited films. Such morphology is favourable for optoelectronic applications, as it minimizes scattering losses and ensures uniform charge transport.

The observed AFM image and corresponding 3D view self organized CdSe nano particle sample A shown in figure 10(a) and (b). The AFM micrograph revealed the as prepared CdSe samples has exhibited a separate dot like morphology of tiny clusters with size ranging of the ordered 2-6nm. Formation of self-organized spherically shaped quantum dots on both the substrates is clearly evidenced. Self-organization of CdSe quantum dots using a chemical bath deposition was a redeeming feature of our study.Selected small area and wide area AFM imaging of several nanocrystalline zinc-blende phase thin film samples of quantum dot sizes 1.6 nm, 2.1 nm, 2.5 nm and 5.5 nm, were performed in the non-contact imaging mode. The individual CdSe quantum dots samples forming an organized array are distinctly resolved in the Figure 10 for the small size nanocrystals CdSe sample-C and Sample-D. The quantum dots of all samples were found to be spherical in shape with an average size of ~5.5nm,
~2.5nm, ~2.1nm and ~1.6nm. The interdot separation was obtained as ~1.25nm to ~2nm in the majority. The average particle sizes estimated by AFM are in close agreement with the average particle size estimated using XRD and TEM as summarized in Table 7. The corresponding particle size distribution histograms obtained from the AFM for sample-A to sample-D have been shown in Figure 11. The particle size distribution has been calculated using the software provided by AFM[79]. It may be remarked that such a self-organized

DOI: 10.22178/acta.26.1.33

ISSN: 2178-7727

growth of semiconductor quantum dots via a room temperature solution route has been demonstrated. Earlier, self-organized growth of semiconductor quantum dots was attempted via vacuum based approaches.

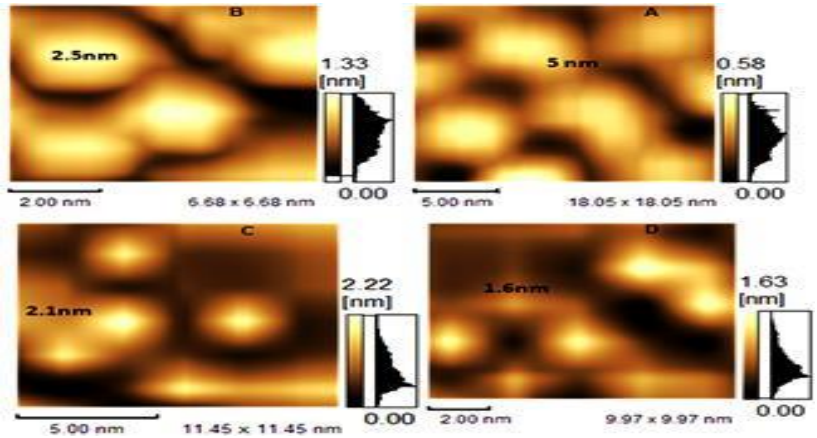

Figure 10. Two-dimensional small area Atomic Force microscope images of CdSe quantum dots sample A (5.5nm), sample B (2.5nm), sample C (2.1nm) and sample D (1.6nm).

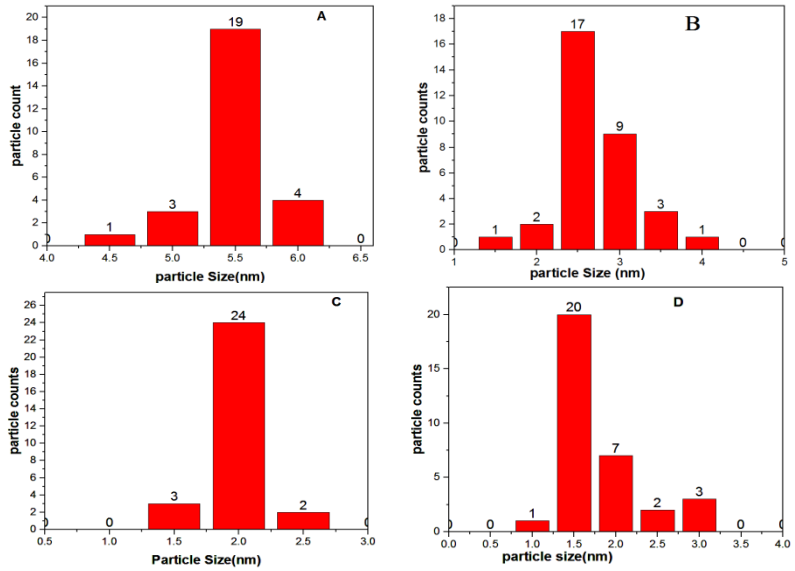

Figure: 11.Observed average particle size distribution histogram for CdSe samples A, B, C and D by AFM.

Table 7 Comparison of estimated average particle size of CdSe quantum dots samples (A)-(D) by AFM, TEM and XRD.

Sample	Particle Size estimated by TEM	Particle Size estimated by XRD	Particle Size estimated by AFM
A	-	5.5	5.5
B	2.5	2.5	2.5
C	-	2.1	2.1
D	1.6	1.6	1.6

Optical Studies

UV–Vis absorption studies

UV–Vis absorption spectra exhibited well-defined excitonic absorption peaks, which were systematically blue-shifted relative to bulk CdSe, confirming strong quantum confinement effects. The optical band gap values increased with decreasing particle size, in accordance with effective mass approximation models. The sharp absorption edges indicate narrow size distribution and minimal defect-related absorption.

The optical absorption spectra of CdSe samples with four different particle sizes have been shown in Figure

DOI: 10.22178/acta.26.1.33

ISSN: 2178-7727

12. Note that in each sample, the sharp rise in the absorption onsets corresponds to the fundamental absorption edges which exhibit systematic blue shift with the reduction in particle size. In addition to the fundamental absorption onset, each of the CdSe nanocrystalline samples (A) to (D) exhibited a second absorption onset on the blue side of the fundamental absorption edge. The 4p orbital of Se constitutes valence band in CdSe while conduction band is composed primarily of 5S electrons of Cd. The optical transitions in CdSe quantum dots would thus involve the S level of the electron **(**conduction band**)** and three p- levels of the holes **(**valence band**)**. Therefore, spin-orbit interaction leads to the occurrence of two electronic transitions one corresponding to the HOMO-LUMO level and another occur at energy higher than the fundamental absorption edge. Moreover, in the case of quantum dots, the continuous band transforms into discrete energy states widely separated from each other which may also give rise to additional features in absorbance.

Alternatively, wide band gap II-VI semiconductor quantum dots using CdTe, CdS and ZnS [80-83] have also been investigated. The absorption edges were identified with the help of the second order derivatives and have been summarized in Table8.

Table 8 A summary of experimentally determined optical absorption edges for CdSe.

Sample	Capp./Se Ratio	Particle Size[nm]	absorption edge nm (eV)	
A	0	5.5	**(**570nm**)**	2.17
B	1:1	2.5	**(**450nm**)**	2.75
C	1.2:1	2.1	**(**422nm**)**	2.93
D	1.5:1	1.6	**(**412nm**)**	3.02

With increasing capping agent molar concentration, the color of the colloidal solution changes from orange-red to orange, yellow and shallow yellow. The range of absorption edge lies between 570 nm to 410 nm which is pronounced blue shift from 712 nm of bulk CdSe band gap [84]. With increasing mercapto-ethanol concentration or decreasing quantum dot size, the range of absorption edges are blue shifted to high energy, which is an evidence for a quantum confinement effect in the CdSe quantum dots samples.

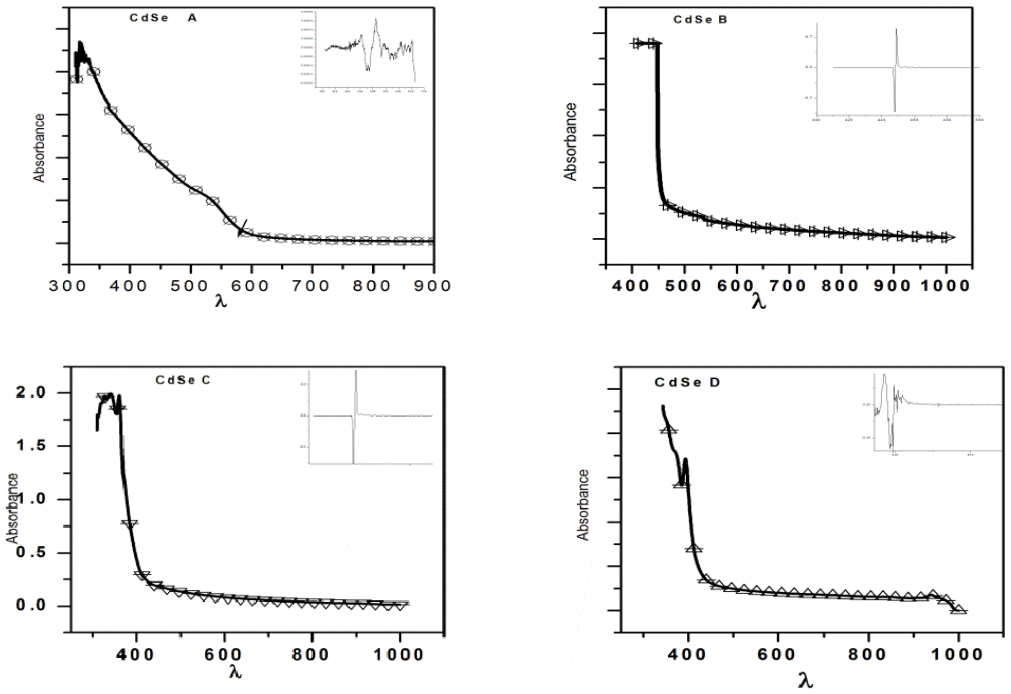

Figure 12.Optical absorption spectra of CdSe quantum dots thin films sample-A Sample-B, Sample-C and Sample-D with corresponding particle size of 5.5, 2.5, 2.1 and 1.6 nm respectively. The second order of fundamental absorption edges showed in the inset corresponding figures.

DOI: 10.22178/acta.26.1.33

ISSN: 2178-7727

The blue shift indicates that the thin film of CdSe consists of nanocrystals with an average radius smaller than Bohr exciton radius ≈ 5.6 nm. It means that our samples have a relatively narrow size distribution [85]. The previous publications record shows that the CdSenanocrystalss with distribution of 10%, shows broadened exciton transition [88,87]. The experimentally determined positions of the absorption edges for all the four samples have been summarized in Table9, along with the corresponding labels.The size dependent blue shifts in the fundamental absorption edge were also calculated by us using existing theoretical models. The TBA and effective mass approximation predict the following relationships for particle size dependent fundamental absorption edge [89].

Table 9 Summary of the observed absorption edges in CdSe. The lowest (fundamental) transition has been leveled

Transitions	Sample A		Difference from lowest Excitation Side E (eV)	Sample B		Difference from lowest Excitation side E (eV)	Sample C		Difference from lowest Excitation side E (eV)	Sample D		Difference from lowest Excitation side E (eV)
	nm.	eV		nm.	eV		nm.	eV		nm.	eV	
$1S_{3/2}$-$1S_e$	570	2.12	0.0	450	2.75	0.0	422	2.92	0.0	412	3.02	0.0
$2S_{3/2}$-$1S_e$	542	2.28	0.11	414	2.96	0.21	389	3.18	0.26	365	3.40	0.38
$1S_{1/2}$-$1S_e$	493	2.52	0.34	390	3.21	0.46	352	3.53	0.61	330	3.76	0.74

The calculated values of the blue shifts using TBA, hyperbolic and EMA theoretical models have been summarized in Table 10. Figure 13 represents the dependence of the blue shifts on particle size calculated using EMA, Hyperbolic band and TB approximations. The experimentally observed blue shifts have also been shown in the figure. Obviously the experimentally observed blue shifts do not agree with any of the calculated values based on the three models.

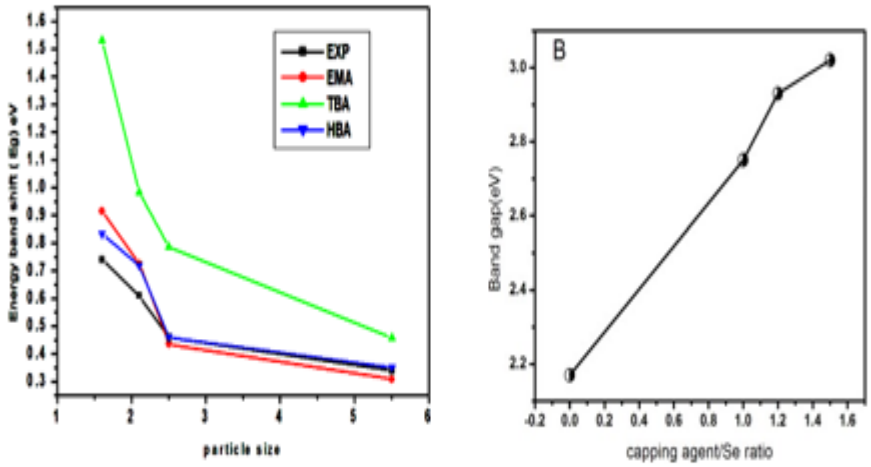

Figure 15. (A) Particle size dependent blue shifts in the fundamental absorption edge by using experimental, EMA, TBA and HBA theoretical models. (B) Capping agent effect on energy band gap.

DOI: 10.22178/acta.26.1.33

ACTA SCIENTIAE

ISSN: 2178-7727

Table: 10 A comparison of the experimentally determined particle size dependent blue shift with the values calculated using effective mass approximation, tight binding approximation and hyperbolic band approximation models.

S.N.	Sample	Particle size (nm)	Energy band shift (Eg) eV				absorption edge (eV)
			EMA	TBA	HBA	Expt.	
1	A	5.5	0.3091	0.4585	0.3504	0.34	2.17
2	B	2.5	0.4352	0.7861	0.4598	0.46	2.75
3	C	2.1	0.7258	0.9840	0.7180	0.61	2.93
4	D	1.6	0.9152	1.5318	0.8335	0.74	3.02

Photoluminescence [PL]

Photoluminescence spectra showed intense band-edge emission with relatively narrow full width at half maximum, reflecting high optical quality. A weaker, broader emission band at longer wavelengths was attributed to surface or trap-state recombination. Core–shell structures exhibited enhanced PL intensity compared to bare CdSe, highlighting the effectiveness of surface passivation in suppressing non-radiative pathways.

Photoluminescence spectroscopy is one of the most common techniques to revel energy structure and surface states. Figure 14 represents the photoluminescence spectra obtained for CdSe sample-A to sample-D deposited by using varying capping agent to selenium ratio. The observed PL emission spectrum consists of a broadband shared with two intense peak at the shorter wavelength side. and relatively two weak peaks at the longer wavelength side in sample A. The all samples-A to sample-D were excited at 380nm and spectrum recorded range from 390nm to 800nm. The photoluminescence spectrum of CdSe quantum dots samples was recorded by Perkin Elemer LS-55, in the visible and NIR regions. The green band is dominant in all the samples studied. Moreover, the intensity of the green band increases with the decreasing crystalline size of the nanocrystals. The small crystal size leads to a large number of surface states in nanocrystals, which play an active role in the optical transition.

Figure 14 also shows the representative multi peak fitted photoluminescence spectrum of nanocrystalline cadmium selenide sample-A, Sample-B, sample-C and sample-D with average particle size 5.5nm, 2.5nm, 2.1nm and 1.6nm respectively. The results of deconvolutions have also been shown in the corresponding Figure 15 by green dotted curves. The deconvoluted spectra could be fitted to four luminescence peaks E1, E2, E3, and E4. The observed peak positions along with the corresponding intensity have been summarized in Table11. The observed peak position in the PL spectra of the CdSe samples exhibited a systematic size-dependent blue shift. All the samples yielded intense PL emissions. However luminescence yield enhanced significantly for quantum dots of smaller particle size. The peak E1 in all the samples were slightly Stoke shifted vis a vis the corresponding fundamental absorption edges of the CdSe quantum dots samples. Peak E1**.** Therefore originate from the band edge luminescence. The Stoke shift systematically increased for sample A **(**dot size 5.5 nm**)** to sample D **(**dot size 1.6 nm**)**. The Stoke shifted emission in quantum dots has been reported by a number of studies. The Stokes shift observed in cadmium selenide quantum dots has been explained by theoretical calculations on fine structure of band edge exciton. Their conclusion is that the initial eight fold band edge exciton state **(**1S3/2-1Se**)** split into five states labelled by the total angular momentum projection by internal crystal field, shape asymmetry and exchange interaction of electron and hole within which the lowest state is optically passive. The luminescence is then Stoke shifted due to efficient relaxation by acoustic phonon emission from higher optically active states. In general the Stoke shift is reported to increase with decreasing particle size. The optically excited electrons are trapped in these surface states followed by the de-exaction to the valence band. As the nanocrystalline size decreases, the surface to volume ratio increase, leading to increase in the intensity of surface related band.The large stoke-shift between optical absorption

DOI: 10.22178/acta.26.1.33

ISSN: 2178-7727

maximum and photoluminescence in quantum dot was observed in several papers and there has been various explanations. First one is the fine structure of band edge exciton. Previous studies suggested that deep states, in particle with nanometre dimensions are mainly associated with Cd^{2+} and Se^{2-} stoichiometric defects and dandling bonds or external atoms like oxygen. [72-78]The peaks E2, E3, and E4 observed in all the PL spectra are positioned towards the longer wavelength side of the corresponding excitonic peaks E1. The difference of energies of peak E2, E3 and E4 from the fundamental edge are practically constant irrespective of the quantum dot size in samples CdSe-A to CdSe-D. These observations therefore indicate that the peaks E2,E3, and E4 could be associated with the recombination mediated by the defects, impurities or vacancies. In all nanocrystalline **(**CdSe-B,CdSe-C and CdSe-D**)**, the defect luminescence E4 was fairly strong, and however the peak E3 was considerably weaker in intensity. The peak E2 in all the 4 samples is very close to the expected luminescence peak position involving Se vacancy therefore it may be attributed to the transition involving Se^{-} vacancy and the highest occupied level. Several studies suggested adsorption of oxygen on many semiconductor surfaces, particularly CdSe can give rise to acceptor and donor type surface states. Other studies suggested that deep states in particles with nanometer dimensions are mainly associated with Cd^{+} and Se^{-} vacancies **(**stoichiometeric defects**)** and dangling bonds or external adatoms [90-100].

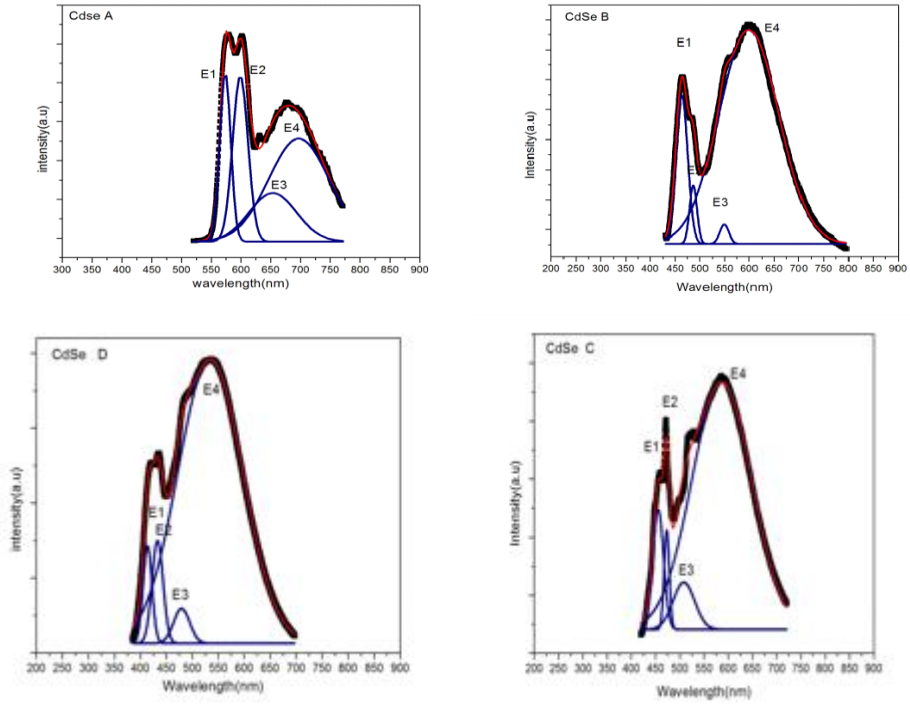

Figure 14. Photoluminescence spectra of CdSe nanocrystalline thin films of samples A, B, C and D with the Gaussian fitting of different 5 peak positions (in blue). Ex=380nm

Table 11 Summary of photoluminescence peak positions and their intensities of CdSe samples A, B, C and D. Excitation = 380 nm.

Sample	Size	Abs.	Photoluminescence Excitation = 380 nm.				Intensity			
			E1	E2	E3	E4	I1	I2	I3	I4
			eV	eV	eV	eV				
Sam A	5.5	570	2.14	2.06	1.95	1.82	7	7	4	5
Sam B	2.5	450	2.66	2.55	2.23	2.06	12	9	13	15
Sam C	2.1	422	2.70	2.63	2.38	2.11	30	40	37	48
Sam D	1.6	412	2.96	2.85	2.55	2.32	124	134	169	196

DOI: 10.22178/acta.26.1.33

ISSN: 2178-7727

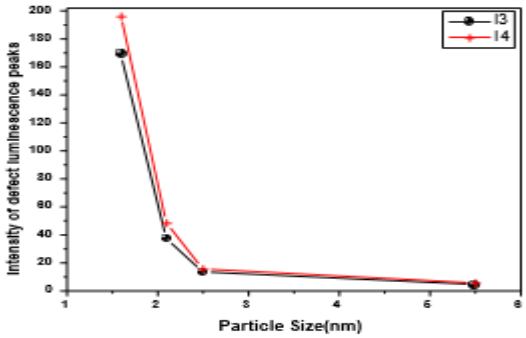

Figure 3.17 Defect luminescence intensity V/S particle size.

3.3. Antimicrobial activity of CdSe quantum dots

In addition to their optoelectronic properties, CdSe quantum dots exhibited notable antimicrobial activity against selected bacterial strains. The antimicrobial performance was evaluated using standard agar diffusion and minimum inhibitory concentration assays against representative Gram-positive and Gram-negative bacteria. The results demonstrated a concentration-dependent inhibition of microbial growth, with smaller-sized quantum dots showing enhanced activity. This behavior can be attributed to the high surface area-to-volume ratio of quantum dots, which facilitates stronger interaction with microbial cell membranes.

The proposed antimicrobial mechanism involves multiple pathways, including the generation of reactive oxygen species under light exposure, disruption of membrane integrity, and interference with intracellular metabolic processes. The release of Cd^{2+} ions at the nanoparticle–cell interface may further contribute to antimicrobial efficacy. Importantly, the observed activity was more pronounced for core–shell structures, suggesting that surface chemistry and stability play a critical role in biological interactions. These findings indicate that CdSe quantum dots synthesized via CBD possess multifunctional potential, combining optoelectronic functionality with antimicrobial activity.

3.4 Conclusion

In this Report, the synthesis of CdSe quantum dots was accomplished by dissolving appropriate amounts of precursor sources for Se- and Cd+ ions in aqueous medium along with the some molar concentration of capping agent. It has been shown that by controlling the capping agent concentration in the growth matrix, one can grow size tunable self-organized CdSequantum dots. The as grown CdSe thin films were found to possess a preferential (111) orientation of the cubic crystal structure. The observed d-values and the calculated lattice constants were in close agreement with the corresponding standard values. It was observed that lattice parameter systematically decreases as the particle size decreases. The reduction in the lattice parameter represents existence of compressive strain in CdSe quantum dots. The average particle size calculated from the Rietveld refinement of the X-ray diffraction pattern reasonably agreed with the TEM. The surface topography of CdSe quantum dots deposited on glass substrate revealed the tendency of CdSe nanocrystallites to exhibit a self-organized growth.

The present study demonstrates the successful synthesis of size-tunable CdSe quantum dots using a simple and scalable chemical bath deposition technique. Comprehensive structural, morphological, and optical analyses confirmed strong quantum confinement effects, high crystallinity, and excellent agreement between different characterization methods. The incorporation of core–shell architectures significantly improved photoluminescence performance by reducing surface-related non-radiative recombination. Additionally, the observed antimicrobial activity highlights the multifunctional nature of CdSe quantum dots and opens avenues for their application in antimicrobial coatings and biomedical devices. Overall, the study establishes chemical bath deposition as a scalable and efficient route for the controlled synthesis of high-quality CdSe quantum dots with tunable optical properties. The strong agreement between structural and optical analyses highlights the self-organized growth behavior of the nanocrystals. These findings contribute to a deeper understanding

DOI: 10.22178/acta.26.1.33

ISSN: 2178-7727

of size-dependent phenomena in semiconductor quantum dots and provide valuable insights for optimizing nanostructures for next-generation optoelectronic and photonic applications (

The fundamental absorption edge measured using optical absorption spectroscopy was found to exhibit a systematic blue shift following reduction in particle size. The blue shift in the absorption edge was shown to be dependent on the size of the CdSe nanocrystallites grown by using successively higher capping agent to Se concentration in the bath. The CdSe films exhibited a broad PL emission band corresponding to band edge luminescence and defect luminescence. Another significant observation from our PL studies was the enhancement in luminescence yield for quantum dots of smaller size presumably due to the organized growth. Our studies thus revealed a relatively simple technique to assemble size tunable and self- organized CdSe quantum dots on substrate using a wet synthesis technique.The Raman spectra of all the three CdSe samples corresponded to sharp peaks corresponding to LO phonon mode and its overtone. The sharp peaks were indicative of CdSe nanocrystals with high monodispersity, crystallinity and good surface conditions. A shift in LO peaks was also observed to decrease in grain size. The broadening and shifting in the peak was assigned to presence of defects in the thin films.

Future work may focus on optimizing surface passivation strategies to further enhance optical efficiency while minimizing potential toxicity. Detailed studies on long-term stability, biocompatibility, and environmentally benign alternatives to cadmium-based systems are also warranted. Furthermore, integrating CdSe quantum dots into device architectures such as photodetectors, sensors, and hybrid nanocomposites represents a promising direction for translating these fundamental findings into practical technologies.

REFERENCES

1. V. L. Colvin, M. C. Schlamp, and A. P. Aiivissatos, Nature, 2,354 (1994).
2. G. Zaiats, D Yanover, R. Vaxenburg, Jenya T. AldonaSashchiuk , Materials 7, 7243(2014).
3. RoozbehHushiarian , Nor AzahYusof , Abdul Halim Abdullah ,ShahrulAinliahAlang Ahmad and Sabo Wada Dutse, Molecules 19, 4355(2014).
4. Nirmal, M. Brus and L. Acc. Chem. Res. 32, 407(1999).
5. H. Weller, Adv. Mater. 5,88(1993).
6. Michalet, F. Pinaud, L. Bentolila, J. Tsay, S. Doose, J. Li, G. Sundaresan, A. Wu,S. Gambhir, S. Weiss. Science. 307, 538(2005).
7. W.C.W. Chan, S.M. Nie. Science. 281,2016(1998).
8. I.L. Medintz, H.T. Uyeda, E.R. Goldman, H. Mattoussi. Nature Mater. 4, 435(2005).
9. J.M. Klostranec, W.C. Chan. Adv. Mater. 18, 1953(2006).
10. A.P. Alivisatos. Nat. Biotechnol22, 47. (2004).
11. D.Y. Wang, A.L. Rogach, F. Caruso. Nano Lett. ,2, 857(2002).
12. B. Farrow, P.V. Kamat. J. Am. Chem. Soc. 131, 11124 (2009).
13. B. Gregg. J. Phys. Chem. B. 107, 4688 (2003).
14. N.A. Gur, M.L Fromer,, A.P. Alivisatos. Science. 310, 462(2005).
15. A.J. Nozik. Physica E. 14, 115(2002).
16. R.D. Schaller, V.I. Klimov. Phys. Rev. Lett. 92, 186601(2004).
17. S. Kumar, G.D. Scholes. MicroshimicaActa. 160, 315(2008).
18. N. Tessler, V. Medvedev, M. Kazes, S.H. Kan, U. Banin. Science. 295, 1506(2002).
19. B.O. Dabbousi, M.G. Bawendi, O. Onitsuka, M.F. Rubner, Appl. Phys. Lett. 66, 1316-(1995).
20. V.L. Colvin, M.C. Schlamp, A.P. Alivisatos. Nature. 370, 354(1994).
21. V.I. Klimov, A. Mikhailovsky, S. Xu, A. Malko, J. Hollingsworth, C. Leatherdale, H. Eisler, M. Bawendi. Science. 290, 314(2000).
22. V.I. Klimov, S.A. Ivanov, J. Nanda, M. Achermann, I. Bezel, J.A. McGuire, A. Piryatinski. Nature. 447, 441(2007).

DOI: 10.22178/acta.26.1.33

ISSN: 2178-7727

23. A.V. Malko, A.A. Mikhailovsky, M.A. Petruska, J.A. Hollingsworth, V.I. Klimov. J. Phys. Chem. B. 108, 5250(2004).
24. B. Fisher, J.-M. Garuge, Y.T. Chan, J. Halpert, M.G. Bawendi. Chem. Phys 318, 71(2005).
25. H.J. Eisler, V.C. Sundar, M.G. Bawendi, M. Walsh, H.I. Smith, V.I. Klimov. Appl.
26. Phys. Lett. 80, 4614(2002).
27. D. Loss, D. DiVincenzo. P. Phys. Rev. A. 57, 120(1998).
28. D.D. Awschalom, D. Loss, N. Samarth, Eds. (Springer-Verlag: Berlin, (2002).
29. S. Lloyd. A potentially realizable quantum computer. Science. 261, 1569(1993).
30. D.P. DiVincenzo. Quantum computation. Science. 270, 255(1995)
31. C.B. Murray, D.J. Norris, M.G. Bawendi.J. Am. Chem. Soc. 115, 8706(1993).
32. M.A. Hines, P. Guyot-Sionnest.J. Phys. Chem. 100, 468(1996).
33. Z.A. Peng, X.G. Peng.J. Am. Chem. Soc. 123, 183(2001).
34. X.G. Peng, J. Wickham, A.P. Alivisatos. J. Am. Chem. Soc. 120, 5343(1998).
35. G.D. Scholes. Adv. Funct. Mater. 18, 1157(2008).
36. X.G. Peng, Adv. Mater. 15, 459(2003).
37. V.I. Klimov. Annu. Rev.Phys. Chem. (2007).58, 635-673
38. A.L. Efros, M. Rosen. Annu. Rev. Mater. Sci. 30,475(2000).
39. D.J. Norris, A.L. Efros, M. Rosen, M.G. Phys. Rev. B. 53, 16347-(1996).
40. M. Nirmal, C.B. Murray, D.J. Norris, M.G. Bawendi. Z. Phys. D. 26, 361(1993).
41. U. Woggon, S.V. Gaponenko. Phys. Status Solidi B. 189, 285-(1995).
42. A.P. Alivisatos. J. Phys. Chem. 100,13226(1996).
43. C. Burda, X.B. Chen, R. Narayanan, M.A. El-Sayed. Chem. Rev. 105, 1025 (2005).
44. M.G. Bawendi, A.R. Kortan, M.L. Steigerwald, L.E. Brus, J. Chem. Phys. 917282(1989).
45. K. Brajesh, H.D. Rai, R.S. Katiyar, M.T.S. Nair, P.K. Nair, A. Mannivannan, J. Appl. Phys.82 1310(1997).
46. F. Trojnek, R. Cingolani, D. Camnoletta, D. Mikes, P. Mikes, P. Nemec, B. Uhlinova, J. Rohovee, P. Maly, J. Cryst. Growth. 209 695(2000).
47. G.D. Scholes. ACS Nano. 2, 523(2006).
48. C. Kittel. Introduction to solid state physics, 7th Edition. (John Wiley and Sons: New York, 1995).
49. N. Ashcroft, N. Mermin. Solid state physics. (Harcourt Brace College Publishers: Fort Worth, 1976).
50. Semiconductor quantum dots physics spectroscopy and applications. Y. Masumoto,
51. T. Takagahara, Eds.(Springer-Verlag: Berlin, 2002).
52. F. Caruso, Ed. (Wiley-VCH: Weinheim, 2004).
53. L. Liu, Z. Zhang, T. Xie, Y.G. Wang, J. Li, Q. Peng, Y. Li. J. Am. Chem. Soc. 131, 16423(2009).
54. J. Jasieniak, C. Bullen, J van Embden, P. MulvaneyJ. Phys.Chem. B. 109, 20665(2005).
55. S.H. Tolbert, A.P. Alivisatos. Science. 265, 373(1994).
56. S.H. Tolbert, A.P. Alivisatos. J. Chem. Phys. 102, 4642(1995).
57. A.B. Sharma, Sudhir Kumar Sharma, M. Sharma, R. K. Pandey and D. S. Reddy, SpectrochimicaActa Part A 72, 285(2009).
58. J Mazher, A K Shrivastav, R V Nandedkar and RK Pandey, Nanotechnology 15 572(2004).
59. D. Pan, Q wang, S jiang and Alijiya, Adv. Mater. 217,(2005). [58]. H M Rietveld refinement ActaCrystallogr, 72, 151 (1987).
60. H M Rietveld refinement J ApplCryst, 2, 65 (1969).
61. R Jose, U N Zhanpeisov, H Fukumura, and I Mitsuru J. Am. Chem. Soc. 128 (2), 629(2006).
62. M B. Mohamed, DTonti, A Chemseddine, and M. Chergui J. Phys. Chem. B, 2005, 109 (21), 10533-10537.
63. T Unger and G. TichyPhys Stat Sol A, 171, 425 (1999).
64. P Thompson, D E Cox and J B Hastings, J ApplCryst, 20, 79 ,(1987).
65. G. Caglioti, A Paoletti, and F P Ricci, Nuclear Instr and Methods, 35, 223 (1958). [65]. General Structure and Analysis System (GSAS): Software Manual by Allen C
66. Larson et al, University of California (1994)

DOI: 10.22178/acta.26.1.33

ISSN: 2178-7727

67. R. M. James, R. L Andrew, J. Nathanael, Stephen J. P and Sandra J. Rosenthal, Applie Material and interfaces. 1 2886(2009).
68. A.K. Arora, and A.K. Ramdas, Phys. Rev. B, 35,4345(1987).
69. A. Baranov, Y. Rakovich, J. Donegan, T. Perova, R. Moore, D. Talapin, A. Rogach,Y. Masumoto, and I. Nabiev, Phy. Rev. B 68, 165306 (2003).
70. F. Comas, C. Trallero-Giner, N. Studart, and G. E. Marques, Phy. Rev. B 65,073303 (2002).
71. R. Gupta, Q. Xiong, G. Mahan, and P. Eklund, Nano Lett. 3, 1745 (2003). [71]. H. Richter, Z. Wang, and L. Ley, Solid State Commun. 39, 625 (1981). [72]. D.J. Norris, A.L Efros and M.G. Bawandi ,Phy. Rev. B , 54 163(1996).
72. A.L Efros, D.J. Norris,M. Nirmal and M.G. Bawandi, , Phy. Rev. B , 54 4843(1996)
73. A L Efros, M Rosen, Kuno M. Phys. Rev. B, [1996], 54 p.4843.
74. M. Nirmal,C.BMurry and M.G. Bawandi, Phys. Rev. B, 50 2293(1994).
75. H. Sharma S. N. Sharma Umesh Kumar V. N. Singh B. R. Mehta and R KakkarJ Mater Sci: Mater Med 20:S123(2009)
76. H. X. Fu, L W Wang and AZunger. Phy Rev B 59, 5568 (1999).
77. D. J. Norris and M G Bawendi, Phy Rev. B, 53 16338(1996).
78. M.Sharma, A.B. Sharma, N. Mishra and R.K. Pandey, “Materials Research Bulletin, 463, 453(2011).
79. B.G. Potter Jr. and J H Simmons, J. Appl. Phys. 68,1219, (1990).
80. Toshihiro Arai, Hidehiko Fujumara, IkuraUmezu, Tsutomu Ogawa and AmericoFujii, Jpn J ApplPhy, 28, 484, (1989).
81. I Yu, T Isobe and M Senna, J Phys Chem. Solid. 57 373 (1996).
82. R N Bhargava D Gallagher, X Hong and A NurmikkoPhy Rev Lett, 72 ,416, (1994). [84]. L. Xu, X. Huang, H. Huang, H. Chen, J. Xu, K. Chen, Jpn. J. Appl. Phys. 37,3491(1998).
83. L.E. Brus, IEEE J. Quantum. Electron, 22, 1909(1986).
84. B. Segall and D.T.F. Marple , Phys. And Chem. Of II-VI compound, Amsterdam 316, (1867).
85. C.B Murry, C.R. Kagan, and M.G. Bawandi, Scienc(1995) 270 1335
86. B Murry, D.J. Norris, and M.G. Bawandi, J. Ame. Chem. Soc.(1993) 115 8706
87. R. H. Bube, and L.A. Barton, J. Phys. Chem. Solids. 29 (1958) 128.
88. R. H.Bube, J. Phys. Chem Solids 1 (1957) 234.
89. D Kaushik, M Sharma, R R Singh, D.K. Gupta, R.K. Pandey, Materials Letters (2006) 60 2994–2997
90. R. H. Bube, J. Chem. Phys. 21 (1953) 1409.
91. E. Guesne, C. Sebenne, M. Balkanski, Surf. Sci. 24 (1971) 18.
92. M.F. Chung and H.E. Farnsworth, Surface. Sci.25 (1972) 321.
93. M.J. Katz, and K.J. Hass, Surface. Sci. 19 (1970) 380.
94. G.A. Somorjai, J. Phys. Chem. Solids. 24 (1963) 175.
95. K. Tanaka, Jpn. J. Appl. Phys. 9 (1970) 1070.
96. N. Chestnoy, T.D. Harris, R. Hull, L.E. Brus, J. Phys. Chem. 90 (1986) 3393.
97. V.A. Smyntyna, Sov. Phys. Semicond. 17 (1983) 424
98. Nirmal M. Norris D.J.Kuno M.Bawendi M. G.. [1995], Phys. Rev. Lett. 75, 3728.
99. Norris D. J. Sacra A. Murray C. B.Bawendi M. G.(1994), Phys. Rev. Lett, 72 2616.

DOI: 10.22178/acta.26.1.33